Journal of Solar Energy Research (JSER)

Journal homepage: www.jser.ut.ac.ir

Using Additional Solar Radiation Absorbers from Local Wood Charcoal to Increase Desalination Efficiency

Muhamad Jafri*, Ben Vasco Tarigan

Department of Mechanical Engineering, Faculty of Sciences and Engineering, Universitas Nusa Cendana
Jl. Adisucipto-Kupang 85001, Indonesia

ARTICLE INFO

Article Type:

Research Article

Received:2025.08.24
Accepted in revised form:2026.06.12

Keywords:
Solar still; Desalination; Natural absorbent; Surface Area Analyzer; Charcoal

A B S T R A C T

The impact of adsorbent media on freshwater productivity and desalination efficiency in solar-powered interfacial desalination systems and terraced ponds is methodically assessed in this work. This experiment used four basins of the same size, but with different absorbent media: Ceiba pentandra charcoal, Gliricidia sepium, Schleicera oleosa, and a control without absorbent media. In addition to analyzing desalination volume and efficiency, the Surface Area Analyzer (SAA) was also tested. The test results showed that, overall, Gliricidia sepium wood charcoal produced a high water volume of 120 mL/h and a desalination efficiency of 21.96%. This happens because Gliricidia sepium charcoal has the highest surface area, pore volume, and pore distribution. Compared with previous reviews that focus on energy requirements, energy savings, and high efficiency in complex pond construction, this paper proposes a simple construction pond that utilizes solar energy, thereby achieving greater efficiency, maximizing desalination volume, and improving the sustainability of the energy-water-environment relationship.

1. Introduction

With urbanization, industrialization, and population growth, demand for freshwater resources is rising. Therefore, we need to utilize alternative water sources [1]. One of the abundant alternative water sources on Earth is seawater. Salt levels in seawater are high, so it cannot be consumed directly for drinking or agricultural purposes. The development of science and technology has enabled various technologies that convert seawater into freshwater suitable for human consumption, such as desalination.

*Corresponding Author Email: muhamad_jafri@staf.undana.ac.id

Cite this article: Jafri, M. and Tarigan, B. Vasco (2026). Using Additional Solar Radiation Absorbers from Local Wood Charcoal to Increase Desalination Efficiency. Journal of Solar Energy Research, 11(2), 3078-3089. doi: 10.22059/jser.2026.391190.1533

DOI: 10.22059/jser.2026.391190.1533

Desalination is the process of making salt-free seawater suitable for human consumption. Reverse osmosis (RO), membrane desalination (MD), humidification-dehumidification (HDH), electro dialysis (ED), multi-effect distillation (MED), and capacitive deionization (CDI) are only a few of the desalination technologies that have been developed. In operation, desalination technology requires an energy source as a driver for the desalination process to occur [2]. The fact that the desalination process requires a significant amount of energy is an important issue, particularly in terms of the sustainability of the process [3].

The energy sources used are generally electrical, mechanical, and thermal energy. However, it has been estimated that about 400 million tonnes of carbon dioxide equivalent have been emitted annually from desalination systems using fossil fuels worldwide over the previous 25 years. Thus, renewable energy sources for desalination, such as solar thermal energy, are necessary and the foremost choice [4]. Drying, space heating, water heating, and saltwater desalting are all common uses of solar thermal energy in households and businesses [5]. Climate change and water shortage are two of today's most pressing issues, and solar-powered water desalination provides a sustainable answer [6].

Hybridization techniques for solar-powered desalination systems achieve acceptable salinity levels (suitable for drinking) while providing high freshwater productivity [7]. Hybrid solar-powered desalination and condenser drives the condensation process [8]. A solar-powered distillation system with a concentrating solar power (CSP) generator can address the urgent need for non-fossil energy sources [9]. Solar desalination systems and photovoltaic (PV) technology address energy and water security issues [10]. Solar-powered desalination photovoltaic (PV) and thermal (T) (PV/T) technology increases energy efficiency [11]. Sound Agitation with Condenser Solar Still (SACSS) and Conventional Solar Still (CSS), SACSS is able to provide air production of 0.38 kg/m²·h, and a peak efficiency of 82% [12], and hybrid magnetic and filtration experiments can lower salinity levels and alleviate the world's water dilemma [13].

Based on the basin construction, solar still desalination basins can be single- or multi-tiered; however, solar stills with multiple-level basins have significantly higher yields [14]. Experiments on double-slope solar distillers (DSSD) basins in the form of double-slope solar distillers Rectangular trough (DSSD-RT), double-slope solar distillers trapezoidal trough (DSSD-TT), and double-slope solar distillers concave trough (DSSD-CT). Shows that the DSSD-CT basin increases the accumulative distillate output by 5.8 L/m².day with an increase of 64.8% compared to the other 2 [15]. Solar desalination with hexagonal pyramid geometry was tested under weather conditions in Ahvaz City, western Iran, resulting in more fresh water and a thermal efficiency of 27.1% [16].

However, freshwater generation from solar collectors still needs to be higher than that of other desalination methods. Therefore, various innovative materials needed in solar collectors have been investigated [17]. Using phase change materials (PCMs), nanofluids, and photovoltaic (PV) panels, as well as innovations in wick materials, can increase productivity by up to 87.4% [18]. A comprehensive analysis of phase change materials (PCMs) and thermoelectric modules (TEMs) shows a productivity increase of 140% each [19]. Energy storage materials and porous materials can be used to boost solar desalination productivity.

Porous materials can absorb other substances, so they are also referred to as adsorbent materials or adsorbing materials used to adsorb fluids (liquid or gas). The phenomenon of adsorption has been known for a long time and has been used in many applications, including solar energy conversion [20], wastewater treatment [21], and water purification [22]. It has also been demonstrated that this kind of combination is effective and raises solar water productivity, like using porous layers of anthracite, nano/PCM, and nano-layers on pipes [23], solutes in the Forward Osmosis (FO) model desalination [24]. The use of nanomaterials/biomaterials to improve the performance of solar desalination systems and their impact on increasing evaporation rates and overall system efficiency [25].

One adsorbent is activated carbon, which has a high adsorption capacity and can be sourced from charcoal or activated charcoal. Carbon (biomass), besides being applied in the biomass-fueled organic Rankine cycle (ORC) for electricity production [26], can also be used as a heat absorber in the desalination process that utilizes activated carbons (Maxsorb III/CaCl2), providing the highest daily water production [27]. The use of different adsorbent materials, including phase change materials, nanofluids, and photovoltaic/thermal (PV/T) systems, tripled freshwater yields and increased energy efficiency, according to an assessment of the results [28]. By improving photothermal absorption, interfacial evaporation,

and sensible heat storage, a more comprehensive and integrated study of biomaterial-based performance enhancement techniques in biomass-derived solar stills raised productivity from 2.3 to 8.8 L/m^2 [29]. The graphite adsorbent (GR) enhances productivity and energy utilization in a solar-driven desalination system, as demonstrated by the development and evaluation of a desalination system that combines a vacuum-tube heat-pipe solar collector with an evaporator-condenser [30].

The average productivity and efficiency of using coal and charcoal as absorbents in a 4645 m^2 square basin were found to be 16.5% and 1.121/m^2, respectively [31]. Charcoal cloth is a good material for use as an absorber/evaporator, according to additional research on the impact of input water flow rate and salinity on distiller productivity, as well as variations in the efficiency of the solar distiller using charcoal cloth as an absorber/evaporator [32]. Gamal (Gliricidia sepium) wood charcoal briquettes were found to be the most productive and efficient when used as absorbents in a single solar still basin [33]. In the solar still reference (SSR) and modified solar still (SSM) basins, natural carbon blocks from fire residues serve as absorbent materials; the results indicate an 8% increase [34]. In a rectangular basin, coconut-shell charcoal briquettes with thicknesses of 10 mm, 20 mm, 30 mm, and 40 mm were used as absorbents throughout the distillation process. According to the findings, coconut shell charcoal briquettes might provide up to 114 milliliters of distilled water per unit area [35]. The solar water distiller is composed of plastic and has a rectangular shape. In addition to offering the benefits of low thermal capacity, light weight, and ease of operation, the bottom is insulated with a layer of sawdust and uses charcoal particles and a wick as an absorber, resulting in a 15% increase in productivity when compared to wick-type distillation [36].

The novelty of this research lies in the use of solar radiation absorbers in the form of charcoal from three types of wood: Ceiba pentandra, Gliricidia sepium, and Schleicera oleosa. These wood-based charcoal raw materials are readily available because they are abundant in areas where desalination technology is used. Charcoal made from these woods has good heat absorption and storage capacity. This study used these materials to assess the volume of desalinated water and the efficiency of solar-powered interface desalination.

2. Materials and Methods

2.1 System description

As shown in Figure 1, this desalination system uses solar radiation as the heat source for evaporation and condensation in the basin. To absorb heat from sun radiation, the two-tiered basin is constructed with a 2 mm black acrylic insulator on the inside and a 12 mm multiplex insulator on the exterior. Seawater vapor is condensed by the basin lid using 2 mm transparent glass. This choice of glass takes into account earlier studies on glass thickness [37] and the optimization of glass thicknesses at 3 mm, 5 mm, and 6 mm [38]. The basin is covered with glass at a 30° inclination angle to the horizontal plane [39]. To direct desalinated water to a measuring cup outside the basin, a ¼-inch plastic pipe is put on the inside of the basin. Charcoal floats in seawater in a basin where evaporation occurs because it absorbs and stores solar heat radiation.

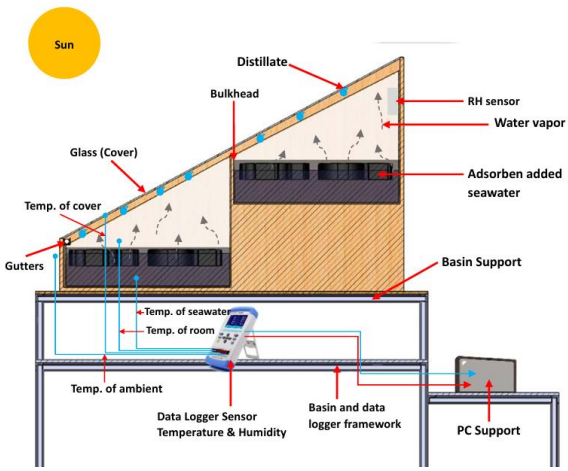

Figure 1. System description solar still desalination basin 2 stage

In addition to the black painted plate at the bottom of the basin, there is also charcoal as an additional absorber and heat storage for solar radiation [34]. Ceiba pentandra, Gliricidia sepium, and Schleichera oleosa are the three types of wood used to make the charcoal. The names of these three types of charcoal are changed to a special code: CP_0 for Ceiba pentandra charcoal (basin 1), GS_0 for Gliricidia sepium charcoal (basin 2), SO_0 for Schleichera oleosa charcoal (basin 3), and without charcoal (basin 4).

Before use, the charcoal was tested using a Surface Area Analyzer (SAA), which operates based on the BET (Brunauer-Emmett-Teller) method and

uses the following equation to determine the surface area of the material [40]:

$$\frac{1}{\left(W\left(\frac{P_0}{P}-1\right)\right)}=\frac{1}{W_m\times C}+\frac{(C-1)(P/P_0)}{W_m\times C} \quad (1)$$

where C is a constant related to the adsorption energy, which indicates the adsorbent/adsorbate interaction, P/Po is the relative pressure, and Wm is the gas volume monolayer capacity at STP. Meanwhile, pore volume and size were determined using the BJH (Barret-Joyner-Halenda) method [40].

2.2 Experimental setup and procedure

Research on multi-level basin solar distillers was conducted to determine optimal desalination volume and efficiency, using appropriate basic specifications and dimensions and incorporating additional solar-heat-absorbing media, such as wood charcoal (Figure 2).

Charcoal chunks and black-painted absorbent plates at the bottom of the basin served as the solar heat absorbers in this investigation. This charcoal was made from three types of dry wood: Kapok (Ceiba pentandra), Gamal (Gliricidia sepium), and Kusambi (Schleichera oleosa). They were found in the nearby area and are quite plentiful. These woods were burnt for three hours at 700°C.

Before testing the use of 3 types of heat-absorbing materials in the desalination process, the material was formed into charcoal. Then, samples from each of the 3 charcoal types were tested for SAA (Surface Area Analyzer). The following steps were used to conduct the testing procedure: 1) Place four basins in a row in an open space and face north. 2) Before adding seawater to the basin, check its salinity. 3) Fill each basin with 30 liters of seawater. 4) Place 3 types of absorbers into three basins with a distribution area of 0.25 m^2, except for the 4th basin. 5) Place a Multi-Channel Temperature Data Logger to measure temperature. 6) To gauge the basin's humidity, install an Elitech RC-4HC moisture data logger. 7) Cover the basin space using glass. 8) To gather and measure the desalinated water, place a measuring cup outside the basin. 9) To gauge the amount of solar radiation, set up an SM26 Solar Power Meter. 10) Points 1 to 9 must be completed before 08:00.

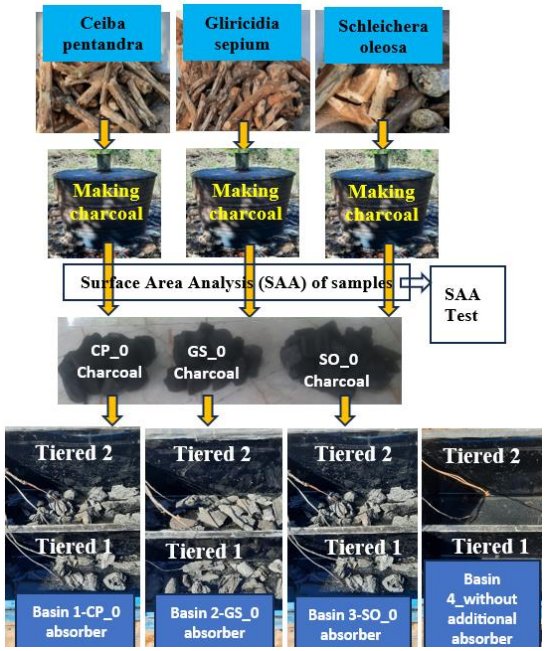

a. b. c. d.

Figure 2. Details basin and absorber (a) Basin 1-CP_0 absorber; (b) Basin 2-GS_0 absorber; (c) Basin 3-SO_0 absorber; (d) without additional absorber.

Temperature measurements were conducted using a Multi-Channel Temperature Data Logger placed on the basin cover glass, seawater surface, and the environment. Sunlight intensity was measured using a Solar Power Meter SM206, and humidity inside the basin was measured using an Elitech RC-4HC. Data were recorded every 30 minutes in reel time.

3. Experimental Results and Discussion

3.1 Surface area analysis

The Surface Area Analyzer (SAA) determines the surface area, pore volume, and pore size of the charcoal adsorbent material derived from three types of wood, coded as CP_0, GS_0, and SO_0. The SAA test was conducted at the Integrated Laboratory of the Islamic University of Indonesia. Nitrogen gas was used for adsorption at a constant pressure and temperature of 77.37 K. The results of the SAA test on the charcoal adsorbent material from three types of wood (Table 1-3).

Table 1. Test result SAA for CP_0 (Ceiba pentandra charcoal)

Results of the Area-Volume Summary	
Surface Area Outcomes	
Multipoint BET	6.0944 m^2/g
BJH adsorption	0.388293 m^2/g
BJH desorption	0.872685 m^2/g
Results of Pore Volume	
BJH total micropore volume of adsorption	0.00108009 cc/g
BJH cumulative micropore volume desorption	0.000875237 cc/g
Total Pre-Volume	0.00385983 cc/g
Results of Pore Size	
Adsorption Pore Radius of BJH	3.09632 nm
Desorption Pore Radius of BJH	1.83729 nm
Pore Size Average	1.26668 nm

Table 2. Test result SAA for GS_0 (Gliricidia sepium charcoal)

Results of the Area-Volume Summary	
Surface Area Outcomes	
Multipoint BET	0.14397 m^2/g
BJH adsorption	0 m^2/g
BJH desorption	0 m^2/g
Results of Pore Volume	
BJH total micropore volume of adsorption	0 cc/g
BJH cumulative micropore volume desorption	0 cc/g
Total Pre-Volume	0.00381403 cc/g
Results of Pore Size	
Adsorption Pore Radius of BJH	1.85161 nm
Desorption Pore Radius of BJH	1.83574 nm
Pore Size Average	52.9836 nm

Table 3. Test result SAA for SO_0 (Schleichera oleosa charcoal)

Results of the Area-Volume Summary	
Surface Area Outcomes	
Multipoint BET	0.12445 m^2/g
BJH adsorption	0.0321363 m^2/g
BJH desorption	0 m^2/g
Results of Pore Volume	
BJH total micropore volume of adsorption	0.000126606 cc/g
BJH cumulative micropore volume desorption	0 cc/g
Total Pre-Volume	0.00251548 cc/g
Results of Pore Size	
Adsorption Pore Radius of BJH	7.8793 nm
Desorption Pore Radius of BJH	1.83742 nm
Pore Size Average	40.4254 nm

The results of SAA testing for the three types of test samples, as shown in tables 1-3, surface area identification was carried out using Nitrogen gas, constant pressure, and a temperature of 77.37 K. For the Brunauer-Emmett-Teller (BET) method, SO_0 has a specific surface area of 0.21445 m^2/g, GS_0, 0.14397 m^2/g. In contrast, CP_0 has a specific surface area of 6.0944 m^2/g.

The amount of Nitrogen adsorbed is also desorbed using the Barret-Joyner-Halenda (BJH) method, which shows that, at CP_0, the amount of Nitrogen adsorbed is 0.388293 m^2/g while desorbed is 0.872685 m^2/g. At GS_0, the Nitrogen adsorbed was 0.0 m^2/g, while it was also desorbed at 0.0 m^2/g. For SO_0, the amount of Nitrogen adsorbed was 0.0321363 m^2/g, while it was desorbed 0.0 m^2/g.

Solar radiation hits the glass covering the basin; some is reflected, while the rest is transmitted to the charcoal surface and collector plate. The charcoal floats on the seawater surface or at the interfacial heating, while the solar collector plate rests at the bottom of the basin. The solar radiation reaching the plate and charcoal surfaces is absorbed, heating the seawater in the basin.

When charcoal floats on the surface of seawater, a wettability phenomenon occurs. This wetness phenomenon causes water to be absorbed into the charcoal through the pores. The heat absorbed by the charcoal turns the absorbed water into steam. The steam is then desorbed onto the charcoal surface. Based on Tables 1, 2, and 3, the pore radius of CP_0 is 3.09632 nm for the adsorption process and 1.83729 nm for the desorption process. The pore radius of GS_0 for the adsorption process is 1.85161 nm, while the desorption process is 1.83574 nm. Meanwhile, the pore radius of SO_0 for adsorption is 7.8793 nm, whereas it is 1.83742 nm for desorption. The pore radius difference between adsorption and desorption for GS_0 is smaller. This indicates that the number of water molecules adsorbed on the charcoal surface is almost equal to the number of vapor molecules desorbed from the charcoal surface onto the inner glass surface.

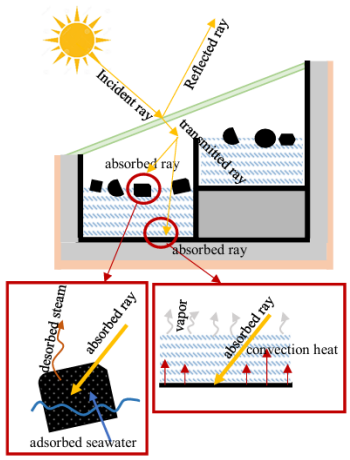

Figure 3. The process of transmitting solar radiation, adsorbed seawater, and desorbed steam

3.2 Solar Radiation Intensity and Environmental Temperature

The measurement data for solar radiation intensity and environmental temperature in each basin are shown in Figure 4 below.

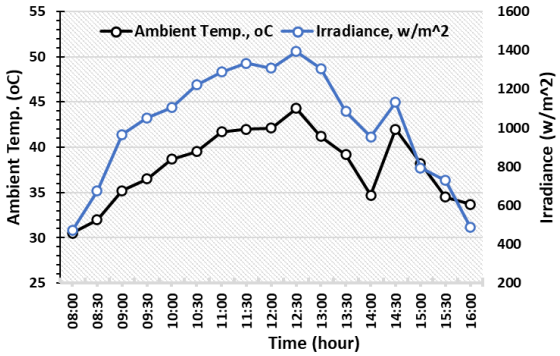

Figure 4. Relationship graph between solar radiation intensity and ambient temperature

Variations in solar radiation intensity are directly proportional to changes in ambient temperature. Increases and decreases in ambient temperature affect the intensity of incoming sunlight. The intensity of solar radiation increased between 8:00 AM and 12:30 PM, raising the ambient temperature. But as the test came to a close at 4:00 PM, the intensity of the sun's radiation progressively dropped, and the surrounding temperature also dropped.

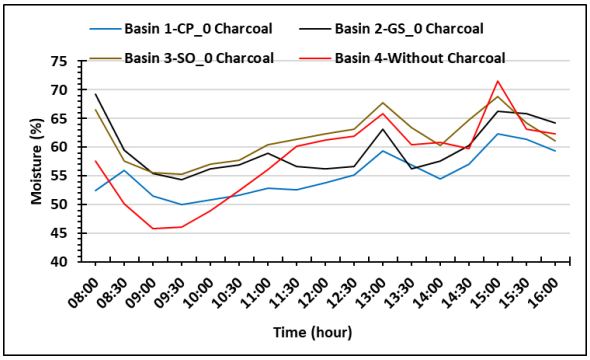

Figure 5. Humidity graph of each room in the basin

Convection within the basin influences the amount of solar energy transported from the inner surface to the charcoal surface, collector plate, and ocean, which in turn influences the humidity inside the basin. The water surface temperature rises as more heat energy is transferred. As shown in Figures 4 and 5, this temperature increase reduces the humidity in the basin. Based on the type of charcoal-based heat absorber of three types of wood, namely CP_0 (basin 1), GS_0 (basin 2), SO_0 (basin 3), and without additional absorber (basin 4), it can be seen that the highest humidity is in the basin using SO_0, followed by GS_0, and CP_0. However, it differs from using a charcoal absorber material, which initially has the lowest humidity. However, from the middle to the end of the test, the humidity increases, approaching SO_0 (basin 3).

3.3 Temperature distribution for each basin

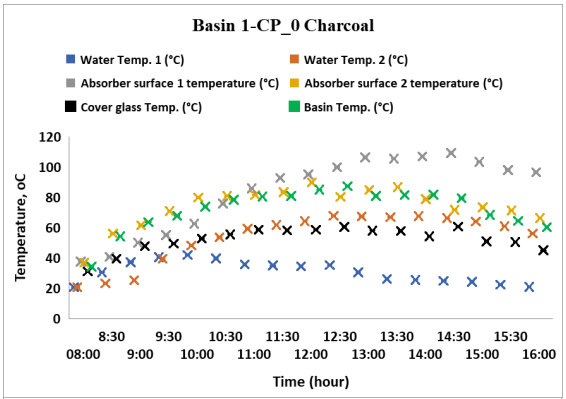

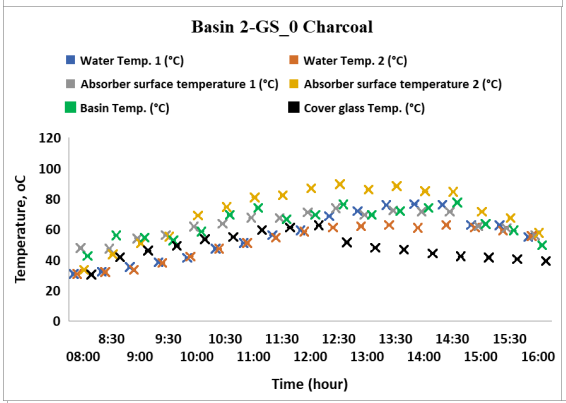

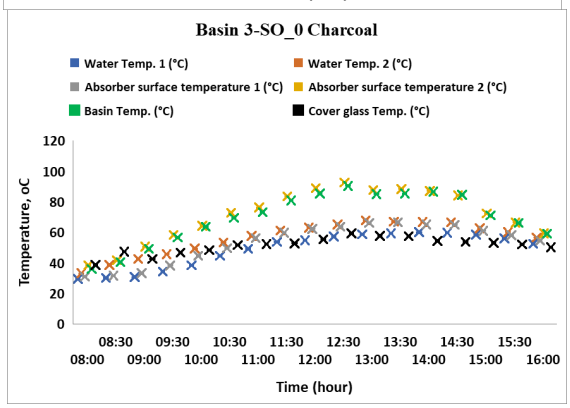

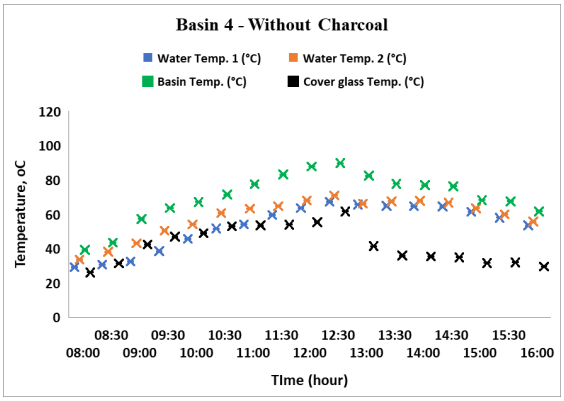

Figure 6. Temperature change at each measurement point for each basin.

Based on Figures 6. a to 6.d, there is a similar trend in temperature change for each point. The temperature initially rose until midday, between 12:00 and 12:30, then decreased until the test ended at 16:00. This is, of course, influenced by the intensity of solar radiation (see Figure 4). Absorbent surface 1, absorbent surface 2, and the basin space had the highest temperatures for each basin. This condition occurs because solar radiation is absorbed and stored in the wood charcoal. At the same time, the basin space experiences latent heat due to evaporation and heat release (condensation) occurring in one room. The lowest temperature occurs at the surface of the basin cover or the cover glass. This is advantageous because the cover glass must be as cold as possible for condensation to occur. The results of seawater salinity measurements before and after our tests are shown below.

Table 4. The results of seawater salinity measurements before and after tests

		pH	TDS (ppm)	Salt% (%ppt)
Before/Pre-testing				
		9,15	3660	0,37
After/Post-testing:				
Basin Charcoal	1-CP_0	6,47	180	0,04
Basin Charcoal	2-GS_0	6,36	176	0,02
Basin Charcoal	3-SO_0	6,50	210	0,04
Basin additional absorber	4-without	6,67	285	0,05

Potential of Hydrogen (pH), Total Dissolved Solids (TDS), and salt content (salinity) are a few desalinated water parameters that can be covered in this paper. Generally, water pH ranges from 0 to 14, with 7 being neutral. The World Health Organization (WHO) states that water with a pH of 6.5 to 8.5 is safe to drink. The pH of water decreases with increasing temperature, indicating an inverse relationship between temperature and pH. This is certainly consistent with surface seawater temperature data in the basin (Figure 6). Meanwhile, regarding dissolved substances from seawater, according to the WHO drinking guidelines (≤ 500 ppm), this is sufficient, with an average across all basins of 212.75 ppm. Meanwhile, the salt content, according to the guidelines, is less than 0.05 ppt (parts per thousand), with an average across the 4 basins of 0.0375 ppt. For Basin 2-GS_0 Charcoal, reductions of 94.59% in salinity and 95.19% in total dissolved solids (TDS) were observed.

3.4 Desalination water production

Every 30 minutes, the volume of desalinated water produced by each basin is measured, and the total desalinated water produced over an 8-hour period from 8:00 am to 4:00 pm is presented in Figures 7 and 8 below.

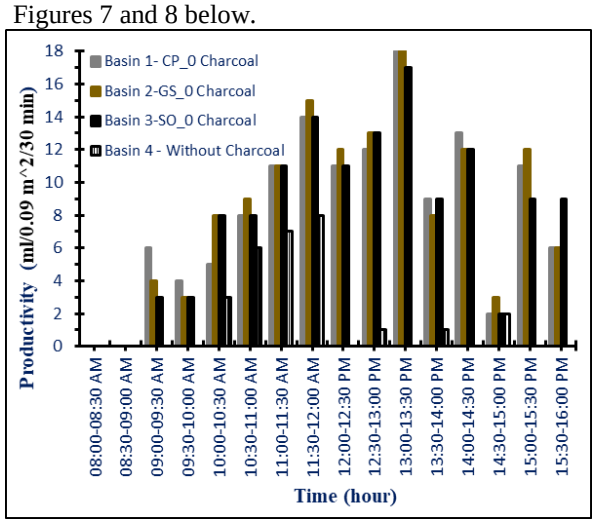

Figure 7. Productivity of desalination water for every basin per half an hour

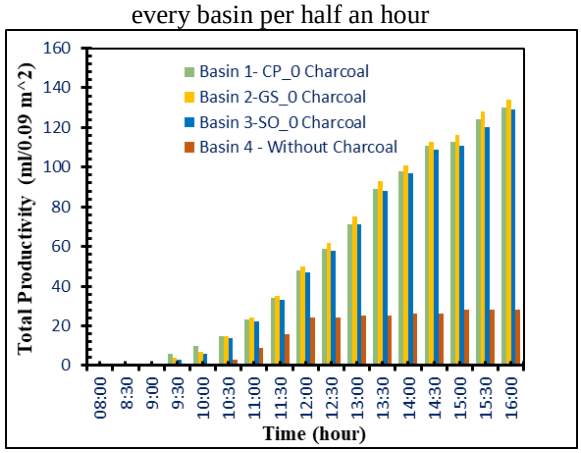

Figure 8. Total desalination each basin

3.5 Uncertainty analysis

Analysis of uncertainty or error range for temperature, humidity, and desalination volume data begins with the tolerance value of each measuring instrument.

Table 5. Accuracy of the measuring instrument used

Variable	
Parameter	Uncertainty
Temperature	0.2℃
Humidity	±1%RH
Volumetric	0,01 mL

The average temperature difference between Basin 1-CP_0 charcoal, Basin 2-GS_0 charcoal, Basin 3-SO_0 charcoal, and Basin 4, without an additional absorber, is 2°C every 30 minutes. With the thermometer's ±0.2°C accuracy, the measurement data is still within the tolerance limit. The humidity-measuring instrument has an accuracy of ±1 % RH. So, with an average difference in humidity values of 5% RH across basins, this also shows it is still within the tolerance limit. Likewise, for the desalination water volume measuring instrument, which has an accuracy of ±0.01 mL and an average difference of 10 mL per data point, this is also within the tolerance limit.

3.6 Rate of Evaporation and Desalination Efficiency

The evaporation rate and desalination efficiency were determined from measured data on temperature, humidity, and solar radiation intensity. The evaporation rate and desalination efficiency were determined from measured data on temperature, humidity, and solar radiation intensity. Before the evaporation rate study, several parameters need to be considered, including the convective heat transfer coefficient (h_{ewg}), the enthalpy of vaporization (h_{fg}), the vapor pressure at the water surface (P_w), and at the inner surface of the glass (P_{gi}). The evaporation rate analysis can use the equation developed by [41].

$$h_{ewg} = \frac{9.15\times10^{-7} h_{wg}(P_w - P_{gi})h_{fg}}{(T_w - T_{gi})} \quad (2)$$

To calculate the convection heat transfer coefficient, it is necessary to know the vapor pressure at the water's surface (P_w) and the inner surface of the basin cover glass (T_{gi}). The formula utilized is the one created by [41].

$$h_{cwg} = 0.884\left[(T_w - T_{gi}) + \frac{(P_w - P_{gi})}{(2016 - P_w)}\right]^{1/3} \quad (3)$$

As for the vapor pressure at the water surface (P_w) and the vapor pressure at the inner surface of the glass (T_{gi}), using the developed equation [42].

$$P_w = 100(0.004516 + 0.0007178T_w - 2.6469\times10^{-6}T_w^{\,2} + 6.944\times10^{-7}T_w^{\,3}) \quad (4)$$

$$P_{gi} = 100(0.004516 + 0.0007178T_{gi} - 2.6469\times10^{-6}T_{gi}^{\,2} + 6.944\times10^{-7}T_{gi}^{\,3}) \quad (5)$$

The results of the analysis of the evaporation heat transfer coefficient from the water surface of the basin to the inner surface of the glass cover are displayed in Figure 8 below.

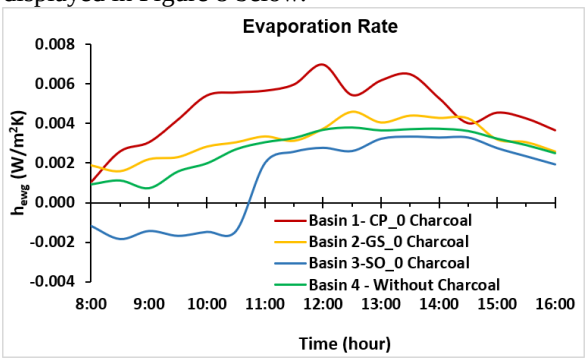

Figure 9. Evaporation rate at each testing time for each basin

From 8:00 a.m. until 12:00 p.m., the evaporation rate for each basin in Figure 9 above shows an increasing tendency; after that, it gradually decreases until the test ends at 4:00 p.m. The evaporation rate rises from morning to afternoon due to an increase in vapor pressure at the water's surface and inside the glass. The amount of charcoal in the basin remains constant, but as the rate of evaporation increases, the depth of the saltwater decreases. The convective heat transfer coefficient, sea level pressure, surface pressure inside the cover glass, enthalpy of evaporation, sea surface temperature, and cover glass temperature all affect the evaporation coefficient, which in turn affects the evaporation rate. This increase surely contributes to the rise in evaporation, given the amount of solar energy the charcoal absorbs and stores. The total heat energy supplied by the sun to the basin via radiation equals the total energy absorbed by the seawater, causing it to evaporate. Furthermore, the total heat energy released by the steam through convection and radiation equals the total energy received by the environment at the surface of the cover glass during condensation. The ability of each charcoal to absorb and store heat varies. More seawater is adsorbed

onto charcoal with larger pores, eventually forming a thin coating on the surface. Simultaneously, the charcoal increases the rate of evaporation by absorbing sunlight and absorbing heat. This also holds true for the test period, which runs from noon until 4:00 p.m. Additionally, Basin 1 has the highest overall evaporation rate, followed by Basin 2, Basin 4, and Basin 3, which have the lowest rates. This happens because, even in the absence of an absorber, basin 1 has a higher absorption rate (6.0944 m^2/g) and a larger surface area as an absorber than basins 2 and 3. BJH was 0.388293 m^2/g when adsorbed and 0.872685 m^2/g when desorbed.

The analysis of the desalination efficiency of four basins, which displays the test variable of charcoal derived from various wood products, comes next. In analyzing the desalination efficiency, the equation used is developed by [43].

$$\eta_d = \frac{m_d \times h_{fg}}{A \times I_s} \times 100\% \quad (6)$$

Heat-absorbing surface area (A), distillate mass (md), enthalpy of evaporation (h_{fg}), and solar radiation intensity (Is) are factors that influence desalination efficiency.

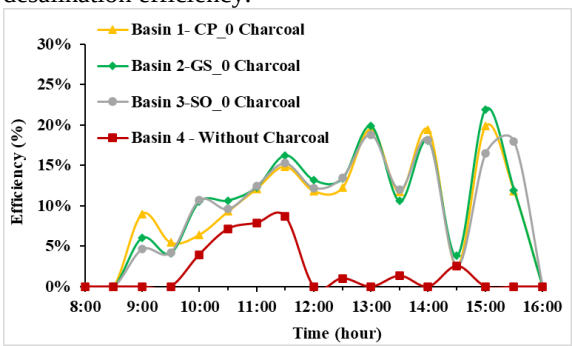

Figure 10. Desalination efficiency for every basin at every test time

A graph of the efficiency change for each basin at each test time is shown in Figure 10. Overall, each basin's efficiency increased from morning to lunch. Additionally, each basin's efficiency dropped between noon and the test's conclusion at 4:00 PM. Additionally, this graph shows that Basin 2 had the highest efficiency, followed by Basins 1, 3, and 4. The graph in Figure 6 shows that Basin 2 had a greater temperature differential between the water surface and the cover glass than the other basins. This led to a low cover glass surface temperature in addition to the high evaporation temperature. A high evaporation temperature and a low condensation temperature will result in a high evaporation rate. The evaporation rate and the distillate mass have a proportional effect on desalination efficiency. Higher mass and evaporation rates, with constant solar radiation intensity and basin area, will result in higher efficiency. The volume and efficiency of desalination increase when the cover glass surface temperature is lower, as this raises the condensation rate and produces more distillate droplets.

4. Conclusions

The use of wood charcoal, Ceiba pentandra, Gliricidia sepium, and Schleichera oleosa as solar radiation absorbers in multilevel desalination tanks affects the volume of desalinated water and desalination efficiency. Wood charcoal, Ceiba pentandra, Gliricidia sepium, and Schleichera oleosa, were analyzed through the Surface Area Analyzer (SAA) process to obtain the characteristics of each wood charcoal, specifically, the values for Surface Area, Pore Volume, and Pore Size. Each wood charcoal has a different value according to the SAA results. Gliricidia sepium wood charcoal produces the maximum volume and efficiency of desalinated water compared to wood charcoal, Ceiba pentandra, Schleichera oleosa, and without wood charcoal. Pore Volume: cumulative adsorption micropore volume: 0 cc/g and cumulative desorption micropore volume: 0 cc/g; Surface Area: (adsorption: 0 m^2/g and desorption: 0 m^2/g); and Pore Size: (adsorption Pore Radius: 1.85161 nm and desorption The results for Gliricidia sepium wood charcoal are as follows: Pore Radius: 1.83574 nm. The heat conductivity of charcoal is influenced by the size of its pores. For charcoal, as a nonmetal, conductivity increases with temperature. Meanwhile, the charcoal's heat capacity depends on the temperature it acquires through heat transfer from solar radiation incident on the basin. As a nonmetal, charcoal's conductivity increases with temperature. Meanwhile, the heat capacity of charcoal depends on temperature, which is determined by heat transfer from solar radiation incident on the container. This study has a limitation: the collection channel is located at the bottom of the basin. This position results in the distillate forming far from the channel, not entering the collection channel, but falling back into the basin seawater. Considering this issue, the next step is to investigate the use of multi-level collection channels within the basin.

Acknowledgments

Through the State University Operational Assistance 2023 National Competitive Research Program, the Directorate of Research, Technology,

and Community Service provided funding for this project.

Nomenclature

A	Heat-Absorbing Surface area (m^2)
C	Constant Associated with Adsorption Energy, Signifying Adsorbent
h_{cwg}	Coefficient of Convection Heat Transfer (W/m^2K),
h_{ewg}	Coefficient of Evaporative Heat Transfer ((W/m^2K))
h_{fg}	Evaporation Enthalpy (kJ/kg)
I_s	The intensity of solar radiation (w/m^2)
m_d	Distillate Mass (kg)
P	The Adsorbing Gas's Equilibrium Pressure (kPa)
P_o	The Adsorbing Gas's Saturated Vapor Pressure (kPa)
P_{gi}	Vapor Pressure on the Surface of Glass (kPa),
P_w	Water Surface Vapor Pressure (kPa),
T_{gi}	Surface Temperature Inside Glass (°C).
T_w	Temperature of the Water Surface (°C),
W	Gas Adsorbed Weight
W_m	Adsorbate Weight as a Monolayer
η_d	Desalination Efficiency (%)

References

[1]Elimelech, M. and W.A. Phillip. (2011). The Future of Seawater Desalination: Energy, Technology, and the Environment. *Science*, *333*(6043), 712–717. https://doi.org/https://doi.org/10.1126/science.1200488

[2]Montazeri, S.M. and G. Kolliopoulos. (2022). Hydrate based desalination for sustainable water treatment: A review. *Desalination*, *537*, 115855. https://doi.org/https://doi.org/10.1016/j.desal.2022.115855

[3]Nagabhooshanam, N., et al. (2025). Sustainable energy integration for seawater desalination. *Toxicological & Environmental Chemistry*, *107*(8), 1582–1605. https://doi.org/10.1080/02772248.2025.2553247

[4]Bundschuh, J., et al. (2021). State-of-the-art of renewable energy sources used in water desalination: Present and future prospects. *Desalination*, *508*, 115035. https://doi.org/10.1016/j.desal.2021.115035

[5]Kumar, A., A.K. Tiwari, and Z. Said. (2021). A comprehensive review analysis on advances of evacuated tube solar collector using nanofluids and PCM. *Sustainable Energy Technologies and Assessments*, *47*, 101417. https://doi.org/https://doi.org/10.1016/j.seta.2021.101417

[6]Madhuri, R.V.S., et al. (2025). Solar energy-driven desalination: A renewable solution for climate change mitigation and advancing sustainable development goals. *Desalination*, *602*, 118575. https://doi.org/https://doi.org/10.1016/j.desal.2025.118575

[7]Alghassab, M.A. (2024). A review of hybrid solar desalination systems: structure and performance. *Water Science and Technology*, *89*(5), 1357–1381. https://doi.org/10.2166/wst.2024.042

[8]Sharshir, S.W., et al. (2025). Using multiple machine learning techniques to enhance the performance prediction of heat pump-driven solar desalination unit. *Desalination and Water Treatment*, *321*, 100916. https://doi.org/https://doi.org/10.1016/j.dwt.2024.100916

[9]Ettouney, H., A. Almutairi, and J. Aljuaidiyah. (2025). Modeling and analysis of large-scale direct contact membrane distillation and parabolic trough concentrated solar power. *Desalination and Water Treatment*, *321*, 100987. https://doi.org/https://doi.org/10.1016/j.dwt.2025.100987

[10]Hmich, M., et al. (2025). Hybrid Solar Desalination System for rural Morocco: Development and performance analysis. *Desalination and Water Treatment*, *321*, 101041. https://doi.org/https://doi.org/10.1016/j.dwt.2025.101041

[11]El-Sayed M. Essa, M., et al. (2025). Developments in solar-driven desalination: Technologies, photovoltaic integration, and processes. *Energy Conversion and Management: X*, *25*, 100861. https://doi.org/https://doi.org/10.1016/j.ecmx.2024.100861

[12]Immanual, R., et al. (2025). Performance enhancement of solar still desalination using sound agitation and condensation: A comparative study. *Desalination and Water*

Treatment, *321*, 100923. https://doi.org/https://doi.org/10.1016/j.dwt.2024.100923

[13]Vellampalli, M.V.S.K. and P. Kuchelar. (2025). A sustainable method of desalination using stacked layer filtration and magnetism. *Desalination and Water Treatment*, *321*, 101033. https://doi.org/https://doi.org/10.1016/j.dwt.2025.101033

[14]Murad, M.E., W.H. Alawee, and H.A. Dhahad. (2024). Advanced techniques for augmenting the performance of double-slope solar stills: A comparative study. *Desalination and Water Treatment*, *320*, 100581. https://doi.org/https://doi.org/10.1016/j.dwt.2024.100581

[15]Boudhiaf, R., et al. (2025). A comparative experimental investigation of rectangular, trapezoidal, and concave basins design to augment the performance of double-slope solar distillers. *Desalination and Water Treatment*, *321*, 100945. https://doi.org/https://doi.org/10.1016/j.dwt.2024.100945

[16]Alamshah, S.A., M. Talebzadegan, and M. Moravej. (2024). Performance Evaluation of Regular Hexagonal Pyramid Three-Dimensional Solar Desalination System: An Experimental Investigation. *Journal of Solar Energy Research*, *9*(2), 1914–1925. https://doi.org/https://doi.org/10.22059/jser.2024.370071.1371

[17]Jamil, F., et al. (2023). Application of advanced energy storage materials in direct solar desalination: A state of art review. *Renewable and Sustainable Energy Reviews*, *186*, 113663. https://doi.org/https://doi.org/10.1016/j.rser.2023.113663

[18]Udoy, S.A., et al. (2024). Advancements in Solar Still Water Desalination: A Comprehensive Review of Design Enhancements and Performance Optimization. *Journal of Solar Energy Research*, *9*(4), 2025–2061. https://doi.org/https://doi.org/10.22059/jser.2025.382301.1464

[19]Khalaf, M.O., M.R. Özdemir, and H.S. Sultan *A Comprehensive Review of Solar Still Technologies and Cost: Innovations in Materials, Design, and Techniques for Enhanced Water Desalination Efficiency*. Water, 2025. **17**, 1515 DOI: https://doi.org/10.3390/w17101515.

[20]da Silva, L. and H.S. Freeman. (2019). Variation in hydrophobic chain length of co-adsorbents to improve dye-sensitized solar cell performance. *Physical chemistry chemical physics : PCCP*, *21*(30), 16771–16778. https://doi.org/https://doi.org/10.1039/c9cp02439e

[21]Rashid, R., et al. (2021). A state-of-the-art review on wastewater treatment techniques: the effectiveness of adsorption method. *Environmental Science and Pollution Research*, *28*(8), 9050–9066. https://doi.org/https://doi.org/10.1007/s11356-021-12395-x

[22]Dotto, G.L. and G. McKay. (2020). Current scenario and challenges in adsorption for water treatment. *Journal of Environmental Chemical Engineering*, *8*(4), 103988. https://doi.org/https://doi.org/10.1016/j.jece.2020.103988

[23]Shoeibi, S., H. Kargarsharifabad, and N. Rahbar. (2021). Effects of nano-enhanced phase change material and nano-coated on the performance of solar stills. *Journal of Energy Storage*, *42*, 103061. https://doi.org/https://doi.org/10.1016/j.est.2021.103061

[24]Reddy, A.S., V.P. Wanjari, and S.P. Singh. (2023). Design, synthesis, and application of thermally responsive draw solutes for sustainable forward osmosis desalination: A review. *Chemosphere*, *317*, 137790. https://doi.org/https://doi.org/10.1016/j.chemosphere.2023.137790

[25]Sharma, M., et al. (2025). Advancement in solar desalination with system innovations, nanomaterials integration, and artificial intelligence applications for sustainability. *Separation and Purification Technology*, 135891. https://doi.org/https://doi.org/10.1016/j.seppur.2025.135891

[26]Heidarnejad, P., et al. (2024). Biomass-Fueled Organic Rankine Cycles: State of the Art and Future Trends. *Energies*, *17*(15), 3788. https://doi.org/https://doi.org/10.3390/en17153788

[27]Ali, E.S., et al. (2025). Cost analysis for solar-powered adsorption desalination-cooling system utilizing improved Maxsorb III adsorbents under Egypt weather conditions. *Alexandria Engineering Journal*, *126*, 341–357. https://doi.org/https://doi.org/10.1016/j.aej.2025.04.038

[28]Ramzy, K., et al. (2026). Advances and challenges in sustainable solar desalination for freshwater production. *Solar Energy*, *304*, 114190. https://doi.org/https://doi.org/10.1016/j.solener.2025.114190

[29]Dhivagar, R. (2026). Biomaterial-based enhancement strategies in solar still desalination: A critical review on progress, challenges, and future perspective. *Desalination*, *626*, 119952. https://doi.org/https://doi.org/10.1016/j.desal.2026.119952

[30]Kusumadewi, R.A., et al. (2026). Hybrid solar adsorption desalination using evacuated tube heat pipe collectors with graphite and biomass adsorbents. *Solar Energy*, *315*, 114765. https://doi.org/https://doi.org/10.1016/j.solener.2026.114765

[31]Okeke, C.E., S.U. Egarievwe, and A.O.E. Animalu. (1990). Effects of coal and charcoal on solar-still performance. *Energy*, *15*(11), 1071–1073. https://doi.org/https://doi.org/10.1016/0360-5442(90)90035-Z

[32]Mahdi, J.T., B.E. Smith, and A.O. Sharif. (2011). An experimental wick-type solar still system: Design and construction. *Desalination*, *267*(2), 233–238. https://doi.org/https://doi.org/10.1016/j.desal.2010.09.032

[33]Jafri, M., B. Tarigan, and D. Adoe. (2024). Solar desalination with charcoal briquettes from plants as an additional absorption sorbent. *Heritage and Sustainable Development*, *6*(1), 183–196. https://doi.org/https://doi.org/10.37868/hsd.v6i1.306

[34]Sadoun, A., et al. (2022). Impact of natural charcoal blocks on the solar still output. *Heritage and Sustainable Development*, *4*(1), 61–66. https://doi.org/https://doi.org/10.37868/hsd.v4i1.80

[35]Tarigan, B.V., M. Jafri, and D.G.H. Adoe. (2024, May) Use of coconut shell charcoal briquettes as PCM seawater distillation. in AIP Conference Proceedings. of Conference. Tangerang, Indonesia.

[36]Naim, M.M. and M.A. Abd El Kawi. (2003). Non-conventional solar stills Part 1. Non-conventional solar stills with charcoal particles as absorber medium. *Desalination*, *153*(1), 55–64. https://doi.org/https://doi.org/10.1016/S0011-9164(02)01093-7

[37]Panchal, H. (2016). Performance Investigation on Variations of Glass Cover Thickness on Solar Still: Experimental and Theoretical Analysis. *Technology and Economics of Smart Grids and Sustainable Energy*, *1*(1), 7. https://doi.org/https://doi.org/10.1007/s40866-016-0007-0

[38]Khechekhouche, A., et al. (2021). Energy, Exergy Analysis, and Optimizations of Collector Cover Thickness of a Solar Still in El Oued Climate, Algeria. *International Journal of Photoenergy*, *2021*(1), 6668325. https://doi.org/https://doi.org/10.1155/2021/6668325

[39]Cherraye, R., et al. (2022). The effect of tilt angle on solar still productivity at different seasons in arid conditions (south Algeria). *International Journal of Ambient Energy*, *43*(1), 1847–1853. https://doi.org/https://doi.org/10.1080/01430750.2020.1723689

[40]Gregg, S.J., K.S.W. Sing, and H.W. Salzberg. (1967, November) Adsorption Surface Area and Porosity. in Journal of The Electrochemical Society. of Conference.: The Electrochemical Society, Inc.

[41]Belessiotis, V., S. Kalogirou, and E. Delyannis, *Solar Distillation—Solar Stills*, in *Thermal Solar Desalination*, V. Belessiotis, S. Kalogirou, and E. Delyannis, Editors. 2016, Academic Press. p. 103–190.

[42]Kalogirou, S.A., *Solar Desalination Systems*, in *Solar Energy Engineering (Second Edition)*, S.A. Kalogirou, Editor. 2014, Academic Press: Boston. p. 431–479.

[43]Zheng, H., *Fundamental Relationships of Heat and Mass Transfer in Solar Seawater Desalination Systems*, in *Solar Energy Desalination Technology*, H. Zheng, Editor. 2017, Elsevier: Amsterdam. p. 173–258.